applied mechanics

MDPI

Article

Morphology-Dependent Resonances in Two Concentric Spheres with Variable Refractive Index in the Outer Layer: Analytic Solutions

Umaporn Nuntaplook [1,2] and John A. Adam [3,*]

[1] Department of Mathematics, Faculty of Science, Mahidol University, Bangkok 10400, Thailand; umaporn.nun@mahidol.ac.th
[2] Center of Excellence in Mathematics, Commission on Higher Education, Bangkok 10400, Thailand
[3] Department of Mathematics and Statistics, Old Dominion University, Norfolk, VA 23529, USA
* Correspondence: jadam@odu.edu

Abstract: In many applications constant or piecewise constant refractive index profiles are used to study the scattering of plane electromagnetic waves by a spherical object. When the structured media has variable refractive indices, this is more of a challenge. In this paper, we investigate the morphology dependent resonances for the scattering of electromagnetic waves from two concentric spheres when the outer shell has a variable refractive index. The resonance analysis is applied to the general solutions of the radial Debye potential for both transverse magnetic and transverse electric modes. Finally, the analytic conditions to determine the resonance locations for this system are derived in the closed form of both modes. Our numerical results are provided with discussion.

Keywords: morphology-dependent resonances; variable refractive index; transverse electric mode; transverse magnetic mode

Citation: Nuntaplook, U.; Adam, J.A. Morphology-Dependent Resonances in Two Concentric Spheres with Variable Refractive Index in the Outer Layer: Analytic Solutions. *Appl. Mech.* **2021**, *2*, 781–796. https://doi.org/10.3390/applmech2040045

Received: 8 July 2021
Accepted: 6 September 2021
Published: 7 October 2021

1. Introduction

Scattering of radiation is a common process that happens in human and animal life. Almost everything we see comes to us indirectly by the scattering of light from objects around us. This leads to many interests in the classical topics of both acoustic and electromagnetic aspects for nanotechnology, transformation optics, fiber optics, metamaterials with negative refractive indices, optical and mechanical problems. These interesting topics are a consequence of the position of the resonance in the electromagnetic scattering in different supporting structures. These resonances are referred to as the morphology-dependent resonances (MDRs), where the electromagnetic energy is temporally trapped inside the particle for a certain period, oscillating back and forth many times before finally tunneling back through the classically forbidden region to the outside world again.

The positions of the resonances can be used to indicate the changes in many aspects of characteristic property such as density, energy, and temperature in the studied structures. The simulations have shown that there will be sharp peak or spike behaviors at the occurring locations of the MDRs as shown in many studies.

Researchers have studied the quasi-bound states, resonance tunnelling, and tunneling times generated by two types of twin symmetric potential barriers. The first is the twin rectangular barrier, and the other is the twin Gaussian-type barrier. They also evaluated the energy levels and widths for both cases. The behavior of the magnitude of wave functions of quasi-bound states as sharp peaks are compared with the regular bound states and the above-barrier state wave function [1].

The recent developments in MDR based sensors for aerospace applications have been reviewed. The concept of a sensor is based on the detection of small shifts of optical resonances, called the Whispering Gallery Mode (WGM). They investigated the MDR in the dielectric spheres. The resonance behaviors are also shown as sharp peaks [2].

Moreover, the conductance through pi-biased chaotic Josephson junctions is accumulated by many orders of magnitude in the short-wavelength regime. They found that mechanism behind this effect can be interpreted as macroscopic resonant tunneling [3].

The behaviors of transmission of the waves through the rectangular barrier when the attractive potential well is present on one or both sides have been studied. They also examined this study for a smoother barrier with a smooth adjacent Woods–Saxon Shape. This work is complementary to the resonant tunneling of objects through the two rectangular barriers. The result can be applied in the design of tunneling devices [4].

The different approach to study the relevant resonance topics is by using the method based on a direct calculation of the Jost matrix together with the Jost solutions of the Schrödinger equation to find a complete solution of one-dimensional Schrödinger equation for any complex energy and any arbitrary potential profile. The total widths of resonances are studied in the square well potential and the two-barrier potential. The resonance energies are demonstrated [5].

The work [6] investigated the group velocity of evanescent waves by using the simulations based on Maxwell equations for both TE and TM modes.

As described here, the MDRs are widely examined in many fields of study. The theory of tunneling is very useful to discuss in resonance phenomena [7].

The basic idea in studying the scattering of electromagnetic waves begins with Maxwell's equations. The process of solving the Maxwell equations in spherical coordinates and solutions has been described in the literature [8,9]. An exact theory of Maxwell's equation was derived and provided the solutions of Maxwell's equations for radially inhomogeneous media and the derivation of the scattering coefficients [10]. Then, B. S. Westcott followed a systematic search by [11] for useful refractive index profiles in spherically inhomogeneous isotropic media [12]. The wave functions are found using the method as that of [13]. He used the technique developed by [11] to derive the refractive index profiles where the wave functions can be expressed in terms of the standard transcendental functions such as hypergeometric, Whittaker or Bessel functions [13]. Several specific refractive index profiles were also studied by [14]. Some relationships of the refractive index profile, the wave number, and the angular momentum were studied by [11–13], who also published a summary of refractive index profiles along with TE and TM solutions corresponding to specific refractive index profiles for spherically layered media.

To determine the conditions to indicate the MDRs locations, only the radial parts of the scattering wave functions need to be used. However, only certain forms of radial parts have been used to derive the conditions to indicate the MDRs locations; most of the wave functions were expressed in terms of the standard transcendental function such as hypergeometric, Whittaker or Bessel functions [13]. The resonance for Mie scattering from a layered sphere was examined by [15,16], who also graphed the contribution of the resonant partial wave to the angle-averaged energy density. In 1993, Johnson developed the theory of morphology-dependent resonances (MDRs) for a spherical particle using the radial Debye potential in the form of Ricatti–Bessel functions and the analogy of quantum-mechanical shape resonances. The exact analytic formulas for predicting the resonances for both real and complex refractive index profiles have been provided [17]. This technique is so called the MDRs technique. He also extended the study of the exact theory of electromagnetic scattering to a heterogeneous multilayer sphere in infinite-layer limit [18,19]. This MDRs technique became very useful in various study.

Many authors graphed internal quantities for a transverse electric and magnetic modes using the MDRs technique for a homogeneous sphere as a function of radius. They considered mostly for the spherical-shaped particles with constant and piecewise-constant refractive index profiles. The cylindrical-shaped particles are also been studied.

The resonances for electric fields distribution in an infinite circular dielectric cylinder with constant refractive index 1.53 and angular momenta 1 to 5 are calculated. The results showed that the internally reflected circumferential waves are located near, but not on the surface [20].

The resonant frequencies and poles for the electromagnetic waves in a dielectric sphere with constant refractive index 1.4 with the size parameters ranging from 1 to 50 have also been studied. The real parts of the calculated poles were used to determine the location of the peaks in the resonance spectrum. The imaginary parts are related to the widths of these peaks [21].

The study of the internal and near-surface scattered field for a spherical particle at resonant conditions are considered. The resonances are examined for various refractive index profiles [22]. The reason that the radial parts for the case of constant and piecewise-constant refractive index profiles have been considered more than the case of variable refractive index is that the radial Debye potential functions for both electric and magnetic fields became identical and simpler to solve comparing to the case of using variable refractive index.

Recently, the topic of morphology dependent resonances (MDRs) has been received much attention for exploring both fundamental research and technological applications. Many researchers have investigated MDR in layered droplets [12,16].

The study of MDRs in homogeneous sphere is now routine. The analysis of spherical particles with more complicated refractive index profiles can be extremely difficult and time consuming. They investigated that the concentration profile of water during sorption in ultraviscous and glassy aerosol particles contains a sharp front that propagates surface to the particle center over time. This result led to the MDR locations corresponding with the type of concentration profile closely matching those of a spherical core–shell structure [23].

The typical resonant TE mode for an incident linearly polarized plane wave in large layered spheres has been investigated by using the theory of Aden and Kerker. The resonance location can be shown as partial wave amplitudes [15].

Another way to study MDRs in a coated sphere is by calculating the volume-averaged source function obtained from Lorenz–Mie theory. The source functions for core and shell contributions can be computed and examined independently. The analytic expressions for the source functions are given [24].

To find the size and composition of core–shell particles using morphology-dependent resonances (MDRs), there are computationally intensive problems due to the large parameter space that needs to be searched during the fitting process. The issue of fitting speed can be solved by developing an algorithm that (i) reduces the multi-dimensional grid search to a one-dimensional search using a least squares method and (ii) implements a new method for calculating MDRs that is much faster than previous methods. They analyzed the best fits for core–shell MDRs across a large range of physically relevant scenarios using noise levels typical for conventional spectroscopic experiments [25].

More recent research studied the resonances of the electromagnetic plane wave in small charged particles. When electrons move freely along the surface of small charged particle, they contribute to scattering phenomena including resonances. These resonances result from excitation of an anti-symmetric surface plasmon at the layer interfaces. The resonance of the radial component of the inner and outer boundaries of the shell are represented as a sharp peak [26].

Other methods to study the behavior of a sharp Lorenz–Mie resonances for a spherical micrometer-sized droplet use the T-matrix [27].

The morphology dependent optical resonances shift (MDR) of a rotating spherical resonator have been analyzed. A shift in its MDR is caused by the centrifugal force acting on the spinning resonator. The MDR shifts of a spinning polydimethylsiloxane (PMDS) microsphere are examined as examples [28].

The researchers developed a new measurement system called 'pulsed 2D-2cLIF-EET' to study temperature fields inside micro-droplets. The MDR and stimulating dye emission are accounted for by using energy transfer [29].

The general solutions of the scattering functions for two concentric spheres when the outer shell has a variable refractive index are derived. The use of these solutions can be

more challenging to analyze the analytic condition to find the resonance location by using the resonance theory [30].

Another recent article [31] studied the MDR of spheres with the discrete dipole approximation (DDA) technique. The DDA simulations can capture the narrow peaks or resonances in the extinction over the size parameters.

The MDRs topics have been studied widely in the objects with spherical in shape. The occurring of MDRs depends on the key conditions—the shape and refractive index of materials. Therefore, the change in the refractive index and radius of microsphere led to the change (shift) in the resonance (MDR) of the microsphere. Many applications of MDR have been shown in the same manner of interpretation [2,12,23,27–30,32]. Lately, the MDR techniques are used to determine the size and composition of core–shell particles. The algorithm for calculating and fitting MDR speed has been developed by reducing the multi-dimensional grid search to one-dimensional search using a least squares method. In this study, the refractive indices are considered as constants, 1.35 and 1.53. The resonance condition for TE and TM modes in this research is known to be [21,25]. The coexistence of high porosity and MDR modes was explored to improve the photocatalytic activity in mesoporous TiO_2 spheres. The MDR modes can be calculated by using the theory of MDR, the coefficients of exponential-like increasing functions have to vanish [33]. The MDRs concept has also been applied to optical-biosensors used in indicating the locations for a high-density photon in micro-droplet [29,33]. The concept also has been used to investigate the size and composition of glassy aerosol microspheres. A core–shell model was used to simplify the analysis of MDR locations during water uptake by high-viscosity aerosol particles. The characteristic equations for the MDRs of such a core–shell particle in case of homogeneous sphere and two concentric spheres are presented by using the refractive indices 1.4 and 1.6 [23].

Moreover, The MDR analysis of a rotating spherical resonator has been analyzed by using optical quality factors. The MDR shifts of a spinning polydimethylsiloxane (PDMS) are found. The interpretation of MDRs was used to design the angular velocity sensor of resonators. The effect of angular velocity on the MDR shifts the spherical resonators that are used as sensing element [28]. The behavior of a sharp Lorenz–Mie resonances or MDR in a spherical micrometer-sized droplet have been studies again by using the superposition T-matrix method. Various values of the size parameters are presented using the constant refractive indices 1.31 and 1.55. Several effects of microscopic inclusions are discussed in a narrow MDR of a micrometer-sized spherical droplet [28]. There are some reviews of the applications of sensors for aerospace based on using the detection of small shifts of optical resonances, which referred to the MDRs. The shift in the resonances (WGM) can be caused by any perturbation to the shape, size or refractive index caused by surrounding environment changing. The MDRs of spheres have been elucidated of a number of theoretical studies. The phenomenon can be described by the analytical techniques using Maxwell's equations and the incident fields in the medium, and the methods and techniques of quantum mechanics, such as the potential well principle among others [2,10,11,17]. The manifestations of MDRs in the elements of the Stokes scattering matrix and their dependence on the refractive index by using the modern visualization techniques was studied. They have found that the scattering matrix can be changed in both magnitude and sign within MDRs using the complex refractive index of a real part of 1.4 and increasing imaginary part from zero to a very small value of 10^{-5}. The potential of using MDRs for optical particle characterization can be significantly improved by measuring ratios of the scattering matrix elements [34].

Although the MDR technique has been widely studied and used to develop many technological applications [2,23,27–29,31–34], the study of MDRs has been mostly done with the particles composed of a constant or piecewise constant refractive index. Both exact conditions and simulation results to find the resonance locations have been investigated. Many approximately spherically symmetric scatters in optical media in our real problems mostly have complex structures, non-constant refractive indices, and are generally not

continuous functions [35]. To indicate the changes in some specific characteristic properties of such complicated structures, it is necessary to determine the exact formulas for predicting the locations of the resonances in various types of objects.

However, the lack of analytical research in this area corresponding with variable refractive index profiles is still a problem. The reason is due to the difficulty of deriving the exact wave scattering solutions, which are required to analyze the analytic solutions to obtain the conditions of resonances for the particles with variable refractive index profiles.

There are many studies in scattering topic dealing with variable refractive index profiles. Most of the wave solutions can be expressed in terms of complex forms of transcendental functions [13]. For example, wave scattering using the variable refractive index called the modified Luneburg lens determined the approximate lens size parameters of morphology-dependent resonances [9]. Using a change of variables method, the scalar radiation potential became the Whittaker function.

Based on the studied research, the exact scattering wave solutions are found in the form of Bessel functions for both TE and TM modes [30]. Moreover, the refractive index profile is of the variable type and can be led to the planoconvex lens, which has the refractive index profile Ar^2, where A is a constant. The MDRs technique was adapted to use wave functions in the form of a Bessel function [17]. By using this technique, the exact formulas can be used to locate the positions of resonances using the variable refractive index as in [30].

Therefore, discovering the exact formulas defining the locations of resonances in the two-concentric sphere when the inner layer has constant refractive index, and the outer has a variable refractive index profile $A(kr)^m$, using the MDRs technique will be investigated here. To do this we consider the wave scattering in the two-concentric sphere when the inner layer has a constant refractive index, and the outer has a variable refractive index profile by [30]. The variable refractive index profile is in the form of $A(kr)^m$, where A and m are the constants, and k is the wave number. The exact radial solutions of the scattering wave solutions are found in the form of Bessel functions for both transverse electric (TE) and transverse magnetic (TM) modes, which is similar to the form that was used to find MDRs' locations by using the MDRs technique developed by [17]. Therefore, the variable refractive index in this work will be considered in the form of $A(kr)^m$. This includes the planoconvex lens, the refractive index profile Ar^2, where A is the constant. With the successful use of the MDRs technique in applying with the wave functions in the form of Bessel function by [17], this gives confidence that the exact formulas defining the MDRs locations using the variable refractive index by [30] can be derived. Since there is no research output yet for the conditions to find the MDRs location in this way, the resulting exact formulas are derived. Therefore, this work will carry out the following results. First, the exact formulas defining the locations of resonances in the two-concentric sphere when the inner layer has constant refractive index, and the outer has a variable refractive index profile $A(kr)^m$, using the MDRs technique. More specifically, the resonance locations will be studied in both transverse electric (TE) and transvers magnetic (TM) modes. Second, the numerical results to find the exact values of the resonance locations by solving the conditions in the exact formulas for both TE and TM modes to confirm the existence of resonances.

The results will be presented to find the resonance locations of the two layers sphere when the inner layer has constant refractive index and the outer layer has variable refractive index of the form $A(kr)^m$. These refractive index profiles can be used as the generalized form of specific refractive index profiles, such as the planoconvex lens. The numerical results will be provided by using the hyperparameter optimization techniques and some numerical methods to find the locations of the resonances using the proposed conditions. The existence of resonances is indicated. The generalized conditions to find the locations of resonances for the two layers sphere with this variable refractive index in the outer layer will be supplied along with the supporting numerical results. Hence, these results can

be used to interpret the important characteristic property in objects that have the similar refractive index profile.

In summary, we investigate the scattering of an electromagnetic plane wave in radially symmetric heterogeneous media. The scattering object is composed of two concentric spheres; the inner layer has constant refractive index and the outer layer has a radially-dependent one. The theory of electromagnetic scattering and the general solutions for both modes (TM and TE) for this model is presented in Section 2. Section 3 describes the derivation of conditions determining the resonance locations for both modes. The work concludes with discussion in Section 4 and conclusions in Section 5.

2. Theory

Consider a two-layer sphere embedded in an infinite uniform medium as shown in Figure 1, regions 1, 2, and 3, respectively, as the radial coordinate increases away from zero. The radius of the inner layer is a, and the outer layer is b (which can be scaled to unity), the center is at origin of the coordinate system, and the refractive index profile in region 2 is considered as a function of the radial coordinate r, defined by $n(r)$. Thus, in region 1, $0 \leq r \leq a$, the refractive index is a constant (n_1). In region 2, $a \leq r \leq b$, the refractive index $n_2(r)$ is defined as $n_3 A(kr)^m$ where A and m are arbitrary constants. In region 3 (exterior to the sphere) $r > b$, and the refractive index, $n_3(r)$ can be any (complex) constant but here is taken to be one. The wave number is $k = 2\pi/\lambda$, where λ is the wavelength of the external incoming electromagnetic plane waves. We consider the case that the sphere is nonmagnetic. The complex time-dependence of the electric field is assumed to be harmonic. As the derivation of equations is developed, many of acronyms and variables are provided in Appendix A in Table A1 to provide readability without flipping back and forth between pages.

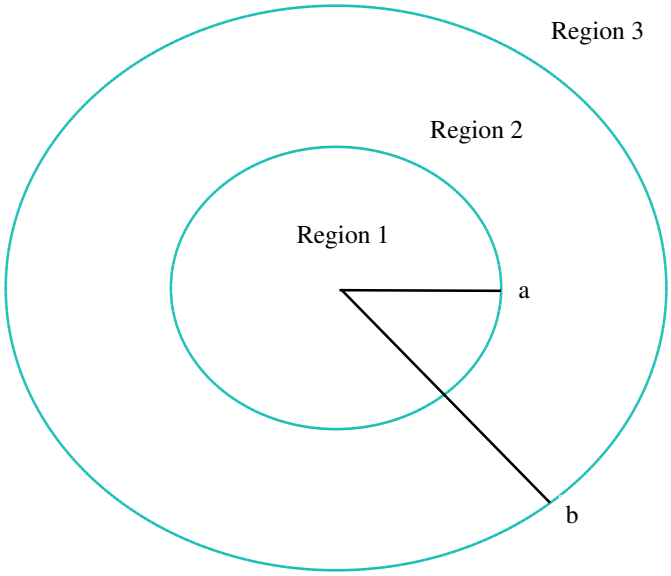

Figure 1. Geometry for a concentric shell particle with variable refractive index. The refractive index of the core in Region 1 is n_1, the refractive index of the shell in Region 2 is n_2, and the refractive index of the outer shell in Region 3 is n_3. The inner radius is a and outer radius is b.

It is known that the solutions of Maxwell's equations can be represented in terms of vector wave functions H describing the transverse magnetic field and a second function B for the transverse electric field [10,17].

$$H(r, \theta, \phi) = \nabla \times [\Psi(r, \theta, \phi)\mathbf{r}], \tag{1}$$

and

$$B(r,\theta,\phi) = \frac{1}{kn^2(r)}\nabla \times \nabla \times [\Phi(r,\theta,\phi)\mathbf{r}]. \tag{2}$$

where r, θ, and ϕ are spherical coordinates, $\mathbf{r}$ is the radius vector, and Ψ and Φ are scalar functions that can be expressed in the following sets of solutions:

$$\Psi_{l,m}(r,\theta,\phi) = \frac{1}{kr}P_l^m(\cos\theta)\exp(im\phi)M_l(r), \tag{3}$$

$$\Phi_{l,m}(r,\theta,\phi) = \frac{1}{kr}P_l^m(\cos\theta)\exp(im\phi)N_l(r), \tag{4}$$

where the $P_l^m(\cos\theta)$ are associated Legendre polynomials. The functions M_l and N_l are the radial Debye potentials, which satisfy the differential equations

$$\frac{d^2M_l}{dr^2} - \frac{2}{n}\frac{dn}{dr}\frac{dM_l}{dr} + \left\{n^2 - \frac{l(l+1)}{r^2}\right\}M_l = 0, \tag{5}$$

$$\frac{d^2N_l}{dr^2} + \left\{n^2 - \frac{l(l+1)}{r^2}\right\}N_l = 0, \tag{6}$$

where l is the angular momentum, the M_l are associated with TM fields, and the N_l functions are associated with TE fields. It is easy to see that if the refractive index $n(r)$ is constant, Equations (5) and (6) are identical. To determine the resonance locations, we focus on the radial parts M_l and N_l [36,37].

2.1. The Wave Solutions for Transverse Magnetic Mode

For the transverse magnetic (TM) mode of this model, we employ the corresponding solutions where $M_{1,l}(r)$, $M_{2,l}(r)$, $M_{3,l}(r)$ are the solutions in regions 1, 2, and 3, respectively, [30].

$$M_{1,l}(r) = n_1 a_l j_l(n_1 kr), \quad \text{for} \quad r < a, \tag{7}$$

$$M_{2,l}(r) = P x_r^{3m/[2(m+1)]}\{A_l j_{\nu-1/2}(x_r) + B_l j_{-(\nu-1/2)}(x_r)\} \quad \text{for} \quad a \le r \le b, \tag{8}$$

$$M_{3,l}(r) = n_3[j_l(n_3 kr) + c_l h_l(n_3 kr)], \quad \text{for} \quad r > b, \tag{9}$$

where a_l, c_l, A_l, B_l are constants, J_ν and $J_{-\nu}$ are Bessel functions of the first kind. The order ν is defined as [38,39]

$$\nu = \frac{1}{(m+1)}\sqrt{l(l+1) + (m+\frac{1}{2})^2}.$$

The parameters

$$P = k^{\frac{1}{2}-m}\left(\frac{A}{m+1}\right)^{1-2m/[2(m+1)]},$$

and

$$x_r = \frac{A}{(m+1)}(kr)^{m+1}.$$

The spherical Bessel functions of the first kind, $j_l(kr)$ is defined as

$$j_l(X) = \sqrt{\left(\frac{\pi}{2X}\right)}J_{l+1/2}, \tag{10}$$

where $J_{l+1/2}$ is a Bessel function of the first kind and half integral order, and $h_l(kr)$ is the spherical Hankel function, defined in terms of regular Hankel function as

$$h_l(X) = \sqrt{\left(\frac{\pi}{2X}\right)} H_{l+1/2} = j_l(X) + ij_{-l}(X), \tag{11}$$

where $H_{l+\frac{1}{2}}$ is the first Hankel function and $j_{-l}(X)$ is defined as

$$j_{-l}(X) = \sqrt{\left(\frac{\pi}{2X}\right)} J_{-(l+1/2)}. \tag{12}$$

2.2. The Wave Solutions for Transverse Electric Mode

For the transverse electric (TE) mode, we suppose the solutions where $N_{1,l}(r)$, $N_{2,l}(r)$, $N_{3,l}(r)$ are the solutions in regions 1, 2, and 3, respectively.

$$N_{1,l}(r) = b_l j_l(n_1 kr) \quad \text{for} \quad r < a, \tag{13}$$

$$N_{2,l}(r) = \frac{S}{(m+1)} x_r^{-m/[2(m+1)]} \{C_l j_{\mu-1/2}(x_r) + D_l j_{-(\mu-1/2)}(x_r)\} \quad \text{for} \quad a \le r \le b, \tag{14}$$

$$N_{3,l}(r) = j_l(n_3 kr) + d_l h_l(n_3 kr), \quad \text{for} \quad r > b, \tag{15}$$

where b_l, d_l, C_l, D_l are constants, J_v and J_{-v} are Bessel functions of the first kind. The order μ is defined as [38,39]

$$\mu = \frac{2l+1}{2(m+1)}.$$

The parameters

$$S = \frac{1}{n_3} k^{1/2} \left(\frac{A}{m+1}\right)^{-1/[2(m+1)]},$$

and

$$x_r = \frac{A}{(m+1)} (kr)^{m+1}.$$

The spherical Bessel functions of the first kind, $j_l(X)$, the Bessel function of the first kind and half integral order, $J_{l+1/2}(X)$, the spherical Hankel function, $h_l(X)$, and the regular Hankel function, $H_{l+\frac{1}{2}}(X)$ are defined as in Equations (10)–(12).

3. Resonance Analysis

As presented in [17], determining the locations of the resonance requires the coefficient of $j_l(kr)$ be zero, i.e., $A_l = 0$ and $1 + c_l = 0$ for TM mode, and $C_l = 0$ and $1 + d_l = 0$ for TE mode. Sections 3.1 and 3.2 show the formulas for all coefficients in both modes.

3.1. TM Mode

To determine the coefficients a_l, c_l, A_l, and B_l, we require that

$$[M_l]_{r=a}, [M_l]_{r=b}, \left[\frac{1}{n^2}\frac{d(rM_l)}{dr}\right]_{r=a}, \left[\frac{1}{n^2}\frac{d(rM_l)}{dr}\right]_{r=b} \tag{16}$$

all be continuous at the boundaries where the refractive index is discontinuous. The four boundary equations at the boundaries $r = a$ and $r = b$ are given by

$$M_{1,l}(a) = M_{2,l}(a), \quad M_{2,l}(b) = M_{3,l}(b),$$

$$\left[\frac{1}{n_1^2}\frac{d(rM_{1,l})}{dr}\right]_{r=a} = \left[\frac{1}{n_2^2}\frac{d(rM_{2,l})}{dr}\right]_{r=a},$$

and

$$\left[\frac{1}{n_2^2}\frac{d(rM_{2,l})}{dr}\right]_{r=b} = \left[\frac{1}{n_3^2}\frac{d(rM_{3,l})}{dr}\right]_{r=b}.$$

The expansions of these equations are presented in Equations (17)–(20), respectively.

$$n_1 a_l j_l(n_1 ka) = P x_a^{3m/[2(m+1)]}\{A_l j_{\nu-1/2}(x_a) + B_l j_{-(\nu-1/2)}(x_a)\}, \tag{17}$$

$$n_3 j_l(n_3 kb) + n_3 c_l h_l(n_3 kb) = P x_b^{3m/[2(m+1)]}\{A_l j_{\nu-1/2}(x_b) + B_l j_{-(\nu-1/2)}(x_b)\} \tag{18}$$

$$\frac{1}{n_1} kaa_l \gamma_l^{(1)}(n_1 ka) = Q x_a^{1/(m+1)}\{A_l \gamma_{\nu-1/2}^{(1)}(x_a) + B_l \gamma_{-(\nu-1/2)}^{(1)}(x_a)\}, \tag{19}$$

$$n_3 kb\{\gamma_l^{(1)}(kb) + c_l \gamma_l^{(3)}(n_3 kb)\} = Q x_b^{1/(m+1)}\{A_l \gamma_{\nu-1/2}^{(1)}(x_b) + B_l \gamma_{-(\nu-1/2)}^{(1)}(x_b)\}, \tag{20}$$

where

$$P = k^{\frac{1}{2}-m}\left(\frac{A}{m+1}\right)^{1-2m/[2(m+1)]}, \quad Q = \frac{1}{An_3^2} k^{\frac{1}{2}-m}\left(\frac{A}{m+1}\right)^{-1/[2(m+1)]},$$

and

$$\gamma_l^{(1)}(X) = \frac{[Xj_l(X)]'}{X}, \quad \gamma_l^{(3)}(X) = \frac{[Xh_l(X)]'}{X},$$

where a prime denotes differentiation with respect to the argument X.

We finally obtain all the coefficients:

$$A_l = \frac{RM}{M\gamma_{\nu-1/2}^{(1)}(x_b) + \gamma_{-(\nu-1/2)}^{(1)}(x_b) - T(Mj_{\nu-1/2}(x_b) + j_{-(\nu-1/2)}(x_b))}, \tag{21}$$

$$B_l = \frac{A_l}{M}, \tag{22}$$

$$a_l = \frac{P x_a^{3m/[2(m+1)]}}{n_1 j_l(n_1 x_0)}\{A_l j_{\nu-1/2}(x_a) + B_l j_{-(\nu-1/2)}(x_a)\}, \tag{23}$$

$$c_l = \frac{P x_b^{3m/[2(m+1)]}\{A_l j_{\nu-1/2}(x_b) + B_l j_{-(\nu-1/2)}(x_b)\} - n_3 j_l(n_3 y_0)}{n_3 h_l(n_3 y_0)}, \tag{24}$$

where $x_0 = ka$ and $y_0 = kb$ are the dimensionless size parameters. The other parameters are defined as

$$J = \frac{x_0 \gamma_l^{(1)}(n_1 x_0) P x_a^{3m/[2(m+1)]}}{n_1^2 j_l(n_1 x_0) Q x_a^{1/(m+1)}}, \quad K = \frac{n_3 y_0}{n_3^2 h_l(n_3 y_0) Q x_b^{1/(m+1)}},$$

$$R = n_3 K[h_l(n_3 y_0)\gamma_l^{(1)}(n_3 y_0) - j_l(n_3 y_0)\gamma_l^{(3)}(n_3 y_0)],$$

$$T = KP x_b^{3m/[2(m+1)]}\gamma_l^{(3)}(n_3 y_0),$$

$$M = \frac{Jj_{-(\nu-1/2)}(x_a) - \gamma_{-(\nu-1/2)}^{(1)}(x_a)}{\gamma_{\nu-1/2}^{(1)}(x_a) - Jj_{\nu-1/2}(x_a)}.$$

3.2. TE Mode

To determine the coefficients b_l, d_l, C_l, and D_l, we require that

$$[N_l]_{r=a}, [N_l]_{r=b}, \left[\frac{d(rN_l)}{dr}\right]_{r=a}, \left[\frac{d(rN_l)}{dr}\right]_{r=b} \tag{25}$$

all be continuous at the boundaries where the refractive index is discontinuous. Note the absence of the n^{-2} term in the above conditions in this case [17]. The four boundary equations at the boundaries $r = a$ and $r = b$ are given by

$$N_{1,l}(a) = N_{2,l}(a), \quad N_{2,l}(b) = N_{3,l}(b),$$
$$\left[\frac{d(rN_{1,l})}{dr}\right]_{r=a} = \left[\frac{d(rN_{2,l})}{dr}\right]_{r=a},$$

and

$$\left[\frac{d(rN_{2,l})}{dr}\right]_{r=b} = \left[\frac{d(rN_{3,l})}{dr}\right]_{r=b}.$$

The expansions of these equations are presented in Equations (26)–(29), respectively.

$$b_l j_l(n_1 ka) = \frac{S}{(m+1)} x_a^{-m/[2(m+1)]} \{C_l j_{\mu-1/2}(x_a) + D_l j_{-(\mu-1/2)}(x_a)\}, \tag{26}$$

$$j_l(n_3 kb) + d_l h_l(n_3 kb) = \frac{S}{(m+1)} x_b^{-m/[2(m+1)]} \{C_l j_{\mu-1/2}(x_b) + D_l j_{-(\mu-1/2)}(x_b)\} \tag{27}$$

$$n_1 ka b_l \gamma_l^{(1)}(n_1 ka) = S x_a^{(2m+1)/(m+1)} \{C_l \gamma^{(1)}_{\mu-1/2}(x_a) + D_l \gamma^{(1)}_{-(\mu-1/2)}(x_a)\}, \tag{28}$$

$$n_3 kb\{\gamma_l^{(1)}(n_3 kb) + d_l \gamma_l^{(3)}(n_3 kb)\} = S x_b^{(2m+1)/(m+1)} \{C_l \gamma^{(1)}_{\mu-1/2}(x_b) + D_l \gamma^{(1)}_{-(\mu-1/2)}(x_b)\}, \tag{29}$$

where

$$S = \frac{1}{n_3} k^{1/2} \left(\frac{A}{m+1}\right)^{-1/[2(m+1)]},$$

and

$$x_r = \frac{A}{(m+1)}(kr)^{m+1}, \quad \gamma_l^{(1)}(X) = \frac{[X j_l(X)]'}{X}, \quad \gamma_l^{(3)}(X) = \frac{[X h_l(X)]'}{X},$$

when a dash denotes differentiation with respect to the argument X.

Finally we obtain all the coefficients:

$$C_l = \frac{N}{PR}, \tag{30}$$

$$D_l = QC_l, \tag{31}$$

$$b_l = \frac{S}{(m+1)} \frac{x_a^{-m/[2(m+1)]}}{j_l(n_1 x_0)} \{C_l j_{\mu-1/2}(x_a) + D_l j_{-(\mu-1/2)}(x_a)\}, \tag{32}$$

$$d_l = \frac{S}{(m+1)} \frac{x_b^{-m/[2(m+1)]}}{h_l(n_3 y_0)} \{C_l j_{\mu-1/2}(x_b) + D_l j_{-(\mu-1/2)}(x_b)\} - j_l(n_3 y_0), \tag{33}$$

again where $x_0 = ka$ and $y_0 = kb$ are the size parameters. The other parameters are defined as

$$M = \frac{n_1 x_0 \gamma_l^{(1)}(n_1 x_0)}{(m+1) j_l(n_1 x_0)} \frac{x_a^{-m/[2(m+1)]}}{x_a^{(2m+1)/(m+1)}},$$

$$N = \frac{n_3 y_0 \gamma_l^{(1)}(n_3 y_0) h_l(n_3 y_0) - n_3 y_0 \gamma_l^{(3)}(n_3 y_0) j_l(n_3 y_0)}{h_l(n_3 y_0)},$$

$$O = \frac{n_3 y_0 \gamma_l^{(3)}(n_3 y_0)}{h_l(n_3 y_0)} \frac{S}{(m+1)} x_b^{-m/[2(m+1)]},$$

$$P = S x_b^{(2m+1)/(m+1)},$$

$$Q = \frac{M j_{\mu-1/2}(x_a) - \gamma_{\mu-1/2}^{(1)}(x_a)}{\gamma_{-(\mu-1/2)}^{(1)}(x_a) - M j_{-(\mu-1/2)}(x_a)},$$

$$R = Q\gamma_{-(\mu-1/2)}^{(1)}(x_b) - \gamma_{\mu-1/2}^{(1)}(x_b) - \frac{QO}{P} j_{-(\mu-1/2)}(x_b) - \frac{O}{P} j_{\mu-1/2}(x_b).$$

4. Discussion

To demonstrate the resonance behavior using the derived analytic condition obtained in the previous section, we consider the potential $V_l(r)$ defined as

$$V_l(r) = \begin{cases} l(l+1)/r^2 + k^2(1-n_1^2), & 0 \le r < a, \\ l(l+1)/r^2 + k^2(1-n_2^2), & a \le r \le b, \\ l(l+1)/r^2, & r > b. \end{cases} \tag{34}$$

The corresponding values of n_1 and n_2 define the behavior of the potential. The characteristic of the potential whether it is attractive, repulsive or some combination of the those two depends on the refractive index values and the wave number. For certain values of the energy level k^2, the phenomenon of resonance will happen. The wave particles will be temporally trapped inside the well or the sharp peak, oscillating back and forth many times before creating the classically forbidden region by tunneling to the outside world.

For various refractive index profiles, the shape of the potential function will be different. The case of constant refractive index can be considered for both increasing functions ($n_1 < n_2$) and decreasing functions ($n_1 > n_2$). The potential for the increasing refractive index profile will have one classically allowed region. On the other hand, there are two classically allowed regions of the potential or double wells for the decreasing refractive index profile.

In this work, we consider the case that the inner layer has a constant refractive index $n_1 = 1.47$, the outer layer has the variable refractive index $n_2 = 2(kr)^{-2}$, outside of the sphere has refractive index $n_3 = 1$, and the angular momentum $l = 40$. The shape of the potential function $V_{40}(r)$ is a single sharp peak as shown in Figure 2. The classically allowed region is the small area inside the sharp peak; outside the sharp peak is called the classical forbidden regions. The behavior of the resonance will occur in the classically allowed regions, then the wave function will continue decay monotonically in the forbidden or barrier regions. The wave function will finally vanish when r tends to infinity.

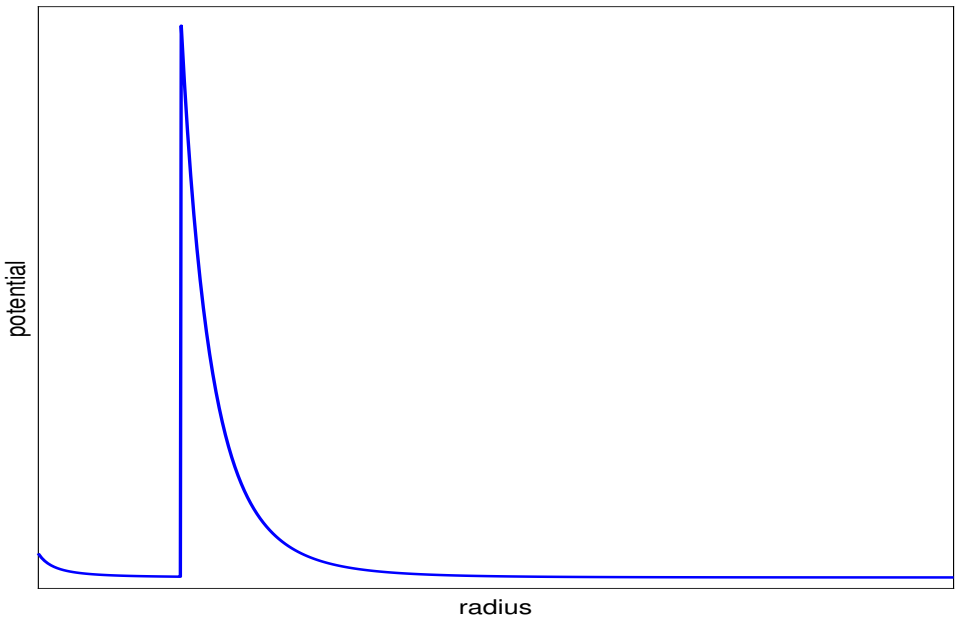

Figure 2. A potential function $V_{40}(r)$ for the case $n_1 = 1.47$, $n_2 = 2(kr)^{-2}$, $n_3 = 1$, and $l = 40$.

The results presented here show the behaviors of the solutions $M_{40}(r)$ for $n_1 = 1.47$, $n_2 = 2(kr)^{-2}$, $n_3 = 1$, and $l = 40$ along with the potential function $V_{40}(r)$. By solving for the size parameters x_0 and y_0 from the derived analytic conditions $A_l = 0$ and $1 + c_l = 0$ for TM mode ($C_l = 0$ and $1 + d_l = 0$ for TE modes), the Gauss–Newton method is applied to search for these size parameters. There are many discrete values that satisfy these necessary conditions. However, we found that only finite values will make the wave function $M_{40}(r)$ stay in the rage of the classically allowed region. Therefore, to obtain the certain values of size parameters to provide resonance phenomena, the range to find these values is strictly determined. The numerical results shown here is obtained by using a-values in the range 0 to 1, and k-values in the range 0 to 10 as example.

The numerical results show that at the size parameters $x_0 = 0.0674664$ and $y_0 = 2.441156$, the solutions $M_{40}(r)$ for $n_1 = 1.47$, $n_2 = 2(kr)^{-2}$, $n_3 = 1$, and $l = 40$ are presented the TM resonance as shown in Figure 3. Only slightly change in the size parameters x_0 and y_0 will make the radial wave function lost the resonance behavior as shown in Figures 4 and 5. Table 1 demonstrates the comparison of the size parameters for the x-value and y-value in each case.

Table 1. The size parameters x-value and y-value for the solutions $M_{40}(r)$ for $n_1 = 1.47$, $n_2 = 2(kr)^{-2}$, $n_3 = 1$, and $l = 40$ of TM mode.

Behavior of the Radial Wave Function	x_0	y_0
On Resonance	0.0674664	2.441156
Below Resonance	0.0574664	2.041156
Above Resonance	0.0874664	2.541156

A typical resonance function is shown in Figure 3 (with the potential function $V_r(40)$ superimposed). The solution $M_{40}(r)$ for $n_1 = 1.47$, $n_2 = 2(kr)^{-2}$, $n_3 = 1$, and $l = 40$ has the TM resonance at $x_0 = 0.0674664$ and $y_0 = 2.441156$. For these values of the energy level, the particles will become temporally trapped inside the sharp peak, keep oscillating back and forth many times and finally tunneling back through the classical forbidden region to the outside particle. Note that this corresponds to an 'almost bound' state because of the very small transmissivity of the wave function into the exterior region 3. This is another way of looking at a resonance; the electromagnetic energy can be considered to be mostly trapped for a period of time until is gradually leaks out of the potential well formed by a

combination of the refractive index and the so-called 'centrifugal potential' [17]. Clearly the TM wave function shown in Figure 3 is effectively trapped close to the surface of the inner sphere. In summary, we have derived the analytic conditions under which such 'virtual bound states' can occur for both polarizations (TM and TE) of the electromagnetic waves.

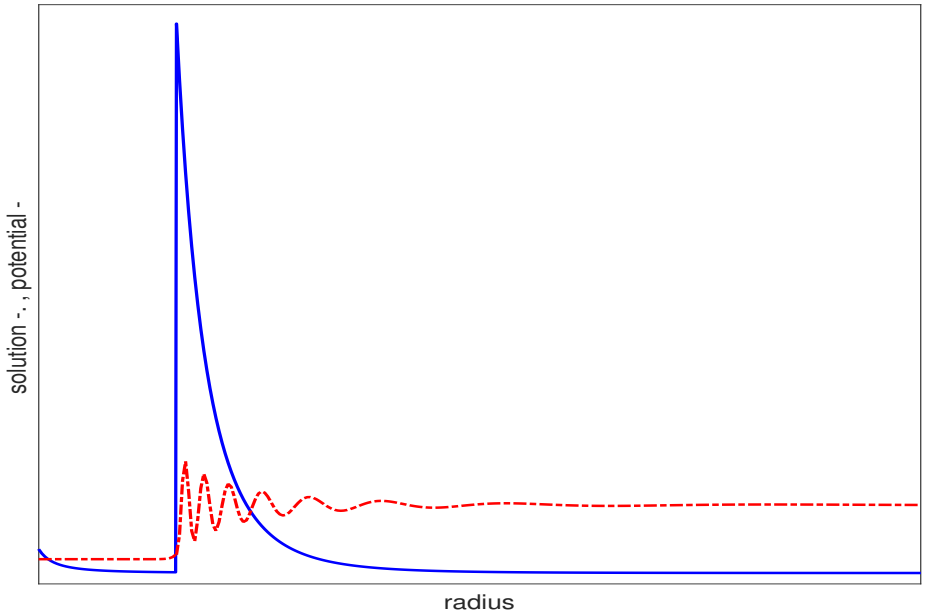

Figure 3. Radial wave functions for TM resonance with $x_0 = 0.0674664$ and $y_0 = 2.441156$. The inner radius is $a = 0.02763707$ and the outer radius $b = 1$. Note how effectively the mode is trapped close to the surface of the inner sphere. Red line (-.) represents the wave solution $M_{40}(r)$; Blue line (-) represents the potential function $V_{40}(r)$.

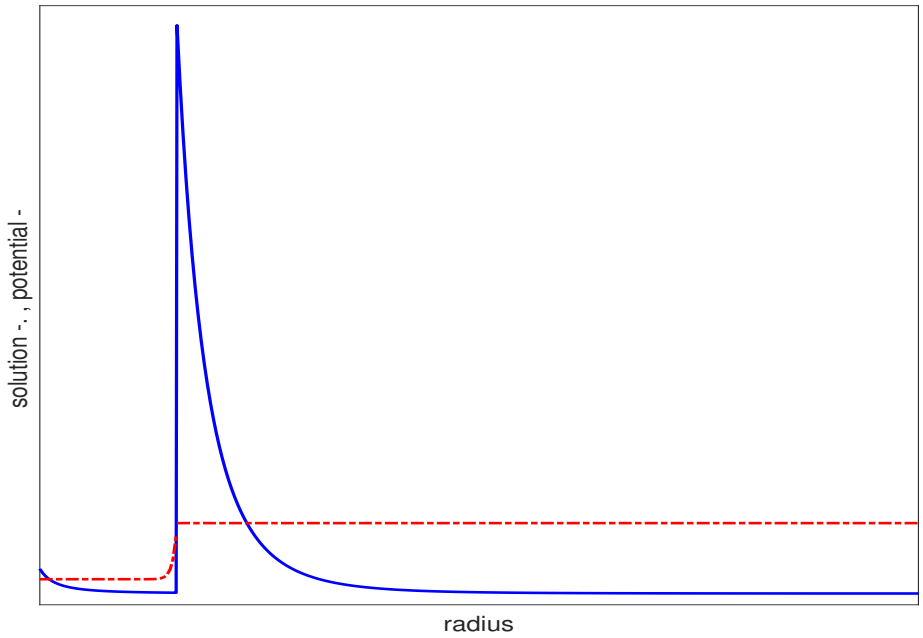

Figure 4. Behavior of the TM wave function in the vicinity of resonance for the case that the size parameters x-value and y-value are slightly below resonance, $x_0 = 0.0574664$ and $y_0 = 2.041156$. The inner layer has a radius $a = 0.02763707$ and the outer layer has a radius $b = 1$. The wave suddenly vanishes before entering the inner region of the surface. Red line (-.) represents the wave solution $M_{40}(r)$; Blue line (-) represents the potential function $V_{40}(r)$.

Figure 4 shows the case that the values of x_0 and y_0 are slightly below the resonance, where $x_0 = 0.0574664$ and $y_0 = 2.041156$. The behavior of the TM wave function suddenly vanishes before entering the allowed region of the sphere and continuing to the outside world without any sharp peaks.

Figure 5 shows the case that the values of x_0 and y_0 are slightly above the resonance, where $x_0 = 0.0874664$ and $y_0 = 2.541156$. The behavior of the TM wave function has an exponential-like increasing manner in the tunneling region, then decays when $r \to \infty$. This case is very similar to the case that the values of x_0 and y_0 are on resonance except that the exponential-like growth in the tunneling region has more higher amplitude than the resonance case and is both inside and outside of the well. The wave is not totally trapped inside the allowed region.

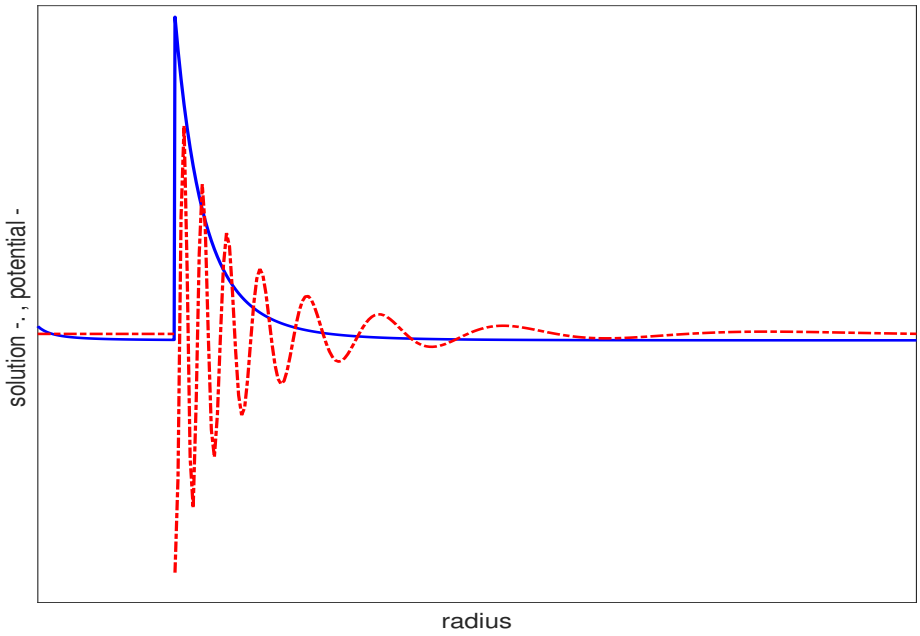

Figure 5. Behavior of the TM wave function in the vicinity of resonance for the case that the size parameters x-value and y-value are slightly above resonance, $x_0 = 0.0874664$ and $y_0 = 2.541156$. The inner radius is $a = 0.02763707$ and the outer radius $b = 1$. Red line (-.) represents the wave solution $M_{40}(r)$; Blue line (-) represents the potential function $V_{40}(r)$.

5. Conclusions

We have presented the derivation of analytic conditions to find the locations of resonances for a two-layer sphere where the inner region has constant refractive index and the outer region has variable refractive index profile of $A(kr)^m$, where A and m are arbitrary constants. Using the resonance analysis, the coefficients of the exponential-like increasing function $j_l(kr)$ in the radial wave functions for both TM and TE modes need to approach zero as $r \to \infty$. This yields the necessary conditions to guarantee that the resonance occurs. The derived analytic conditions to determine the resonance locations have been investigated here as the parameters $A_l = 0$ and $1 + c_l = 0$ for TM mode, and $C_l = 0$ and $1 + d_l = 0$ for TE modes. Since we are dealing with the variable refractive index profile, it may not lead to a total bound state as in the case of constant refractive index profiles.

For future work, there are many useful variable refractive indices that can be applied by using this resonance analysis. Other analytic solutions [11–13] still await investigation. These provide many interesting cases for future study. However, the analysis may encounter obstacles when dealing with singular refractive index profiles. The unstructured mesh finite element method can still be applied, however, especially in the case that the analytic forms of conditions to find the resonance locations are not provided.

Author Contributions: The authors have an equal work. All authors have read and agreed to the published version of the manuscript.

Funding: This research received no external funding.

Institutional Review Board Statement: Not applicable.

Informed Consent Statement: Not applicable.

Data Availability Statement: Not applicable.

Conflicts of Interest: The authors declare no conflict of interest.

Abbreviations

The following abbreviations are used in this manuscript:

MDR	Morphology-dependent resonance
WGM	Whispering gallery mode
TE	Transverse Electric
TM	Transverse Magnetic

Appendix A

Table A1. The Consolidated table of variable definitions.

Variable	Definition
a	radius of the inner layer of the two concentric spheres in Figure 1
b	radius of the outer layer of the two concentric spheres in Figure 1
r, θ, ϕ	the spherical coordinates of the two concentric spheres in Figure 1
n_1, n_2, n_3	refractive indices in Region 1, 2, and 3 of the two concentric spheres in Figure 1
k	wave number of the external incoming electromagnetic plane waves
λ	wavelength of the external incoming electromagnetic plane wave
H	vector wave function for transverse magnetic field
B	vector wave function for transverse electric field
Ψ, Φ	scalar functions of the vector wave function
l	angular momentum
M_l, N_l	radial Debye potentials
J_ν	Bessel function of the first kind of order ν
j_ν	spherical Bessel function of the first kind of order ν
h_ν	spherical Hankel function of order ν
$V_l(r)$	potential function
x_0, y_0	size parameters

References

1. Uma Maheswari, A.; Prema, P.; Mahadevan, S.; Shastry, C.S. Quasi-bound states, resonance tunnelling, and tunnelling times generated by twin symmetric barriers. *Pramana* **2009**, *73*, 969. [CrossRef]
2. Adamovsky, G.; Otugen, M.V. Morphology-dependent resonances and their applications to sensing in aerospace environments. *J. Aerosp. Comput. Inf. Commun.* **2008**, *5*, 409–424. [CrossRef]
3. Goorden, M.C.; Jacquod, P.; Weiss, J. Superconductivity-induced macroscopic resonant tunneling. *J. Phys. Rev. Lett.* **2008**, *100*, 067001. [CrossRef]
4. Mahadevan, S.; Prema, P.; Agarwalla, S.K.; Sahu, B.; Shastry, C.S. Resonance-like tunneling across a barrier with adjacent wells. *Pramana* **2006**, *67*, 401–413. [CrossRef]
5. Rakityansky, S.A. Unified treatment of bound, scattering, and resonant states in one-dimensional semiconductor nanostructures. *Phys. Rev. B* **2003**, *68*, 195320. [CrossRef]
6. Parbero, A.P.; Hernandez-Fegueroa, H.E.; Recami, E. Propagation speed of evanescent modes. *Phys. Rev. E* **2000**, *62*, 8628. [CrossRef] [PubMed]
7. Razavy, M. *Quantum Theory of Tunnelling*; World Scientific: Singapore, 2003.
8. Tai, C.T. Some wave functions and potential functions pertaining to spherically stratified media. *J. Res. Natl. Bur. Stand.-D. Radio Propag.* **1963**, *67*, 199–202. [CrossRef]
9. Lock, J.A. Scattering of an electromagnetic plane wave by a Luneburg Lens. II. wave theory. *J. Opt. Soc. Am. A* **2008**, *25*, 2980–2990. [CrossRef] [PubMed]

10. Wyatt, P.J. Scattering of electromagnetic plane waves from inhomogeneous spherically symmetric objects. *Phys. Rev.* **1962**, *127*, 1837–1843. [CrossRef]
11. Heading, J. Refractive index profiles based on the hypergeometric equation and the confluent hypergeometric equation. *Proc. Camb. Philos. Soc.* **1965**, *61*, 897. [CrossRef]
12. Westcott, B.S. Exact solutions for electromagnetic wave propagation in spherically stratified isotropic media. *Proc. Camb. Phil. Soc.***1968**, *64*, 227. [CrossRef]
13. Sharaf, A.L. Exact solutions for fields of electric type in spherically stratified isotropic media. *Proc. Camb. Phil. Soc.* **1968**, *66*, 119. [CrossRef]
14. Nomura, Y.; Takatu, K.I. Exact solutions for fields of electric type in spherically stratified isotropic media. *Sci. Rep. Res. Inst. Tohoku Univ. Ser.* **1966**, *A7*, 1127.
15. Hightower, R.L.; Richardson, C.B. Resonant Mie scattering from a layered sphere. *Appl. Opt.* **1988**, *27*, 4850–4855. [CrossRef]
16. Lock, J.A. Interference enhancement of the internal fields at structural scattering resonances of a coated sphere. *Appl. Opt.* **1990**, *29*, 3180–3187. [CrossRef] [PubMed]
17. Johnson, B.R. Theory of morphology-dependent resonances: Shape resonances and width formulas. *J. Opt. Soc. Am.* **1993**, *A10*, 343–352. [CrossRef]
18. Johnson, B.R. Light scattering by a multilayer sphere. *Appl. Opt.* **1996**, *35*, 3286–3296. [CrossRef] [PubMed]
19. Johnson, B.R. Exact theory of electromagnetic scattering by a heterogeneous multilayer sphere in the infinite-layer limit: effective-media approach. *J. Opt. Soc. Am. A* **1999**, *16*, 845–852. [CrossRef]
20. Owen, J.F.; Chang, R.K.; Barber, P.W. Internal electric field distributions of a dielectric cylinder at resonance wavelengths. *Opt. Lett.* **1981**, *6*, 540–542. [CrossRef] [PubMed]
21. Conwell, P.R.; Barber, P.W.; Rushforth, C.K. Resonant spectra of dielectric spheres. *J. Opt. Soc. Am.* **1984**, *A1*, 62–67. [CrossRef]
22. Chylek, P.; Pendelton, J.D.; Pinnick, R.G. Internal and near-surface scattered field of a spherical particle at resonant conditions. *Appl. Opt.* **1985**, *24*, 3940–3942. [CrossRef]
23. Moridnejad, A.;Preston, T.C.; Krieger, U.K. Tracking water sorption in glassy aerosol particles using Morphology-dependent resonances. *J. Phys. Chem. A* **2017**, *121*, 8176–8184. [CrossRef] [PubMed]
24. Kaiser, T.; Lange, S.; Schweiger, G. Structural resonances in a coated sphere investigation of the volume-averaged source function and resonance positions. *Appl. Opt.* **1994**, *33*, 7789–7797. [CrossRef]
25. Vennes, B.; Preston, T.C. Calculating and fitting morphology-dependent resonances of a spherical particle with a concentric spherical shell. *J. Opt. Soc. Am. A* **2019**, *36*, 2089–2103. [CrossRef]
26. Markoš, P.; Kocifaj, M.; Kundracik, F.; Videen, G. Electromagnetic resonances observed in small, charged particles. *J. Quant. Spectrosc. Radiat. Transf.* **2021**, *272*, 107798. [CrossRef]
27. Mishchenko, M.I.; Liu, L; Mackowski, D.W. Morphology-dependent resonances of spherical droplets with numerous microscopic inclusions. *Opt. Lett.* **2014**, *39*, 1701–1704. [CrossRef] [PubMed]
28. Ali, A.R.; Loppolo, T. Effect of angular velocity on sensors based on morphology dependent resonances. *Sensors* **2014**, *14*, 7041–7048. [CrossRef]
29. Palmer, J.; Reddemann, M.A.; Kirsch, V.; Kneer, R. Applying 2D-2cLIF-EET thermometry for micro-droplet internal temperature imaging. *Exp. Fluids* **2018**, *59*, 51. [CrossRef]
30. Levine, S.; Kerker, M. Scattering of electromagnetic waves from two concentric spheres, when outer shell has a variable refractive index. ICES Electromagnetic. In *Proceedings of the Interdisciplinary Conference Held at Clarkson College of Technology, Potsdam, Germany, August 1962*; The MacMillan Company, pursuant to a special arrangement with Pergramon Press: Oxford, UK, 1963; pp. 37–46.
31. Zhu, Y.; Liu, C.; Yurkin. M.A. Reproducing the morphology-dependent resonances of spheres with the discrete dipole approximation, *Opt. Express* **2019**, *27*, 22827–22845. [CrossRef]
32. Kalume, A.; Wang, C.; Pan, Y.-L. Optical-trapping laser techniques for characterizing airborne aerosol particles and its application in chemical aerosol study. *Micromachines* **2021**, *12*, 466. [CrossRef] [PubMed]
33. Kalyan, I.; Krishnamurthy, C.V. Morphology dependent resonance modes in highly porous TiO_2 microspheres. *J. Appl. Phys.* **2018**, *124*, 133102. [CrossRef]
34. Mishchenko, M.I.; Lacis, A.A. Manifestations of morphology-dependent resonances in Mie scattering matrices. *Appl. Math. Comput.* **2000**, *116*, 167–199. [CrossRef]
35. Adam, J.A.; Laven, P. Rainbows from inhomogeneous transparent spheres: A ray-theoretic approach. *Appl. Opt.* **2007**, *46*, 922–929. [CrossRef] [PubMed]
36. Adam, J.A. *Scattering of Electromagnetic Plane Waves in Radially Inhomogeneous Media: Ray Theory, Exact Solutions and Connections with Potential Scattering Theory*; Light Scattering Reviews 9; Springer Praxis Books; Springer: Berlin/Heidelberg, Germany, 2015; pp. 101–132.
37. Nuntaplook, U.; Adam, J.A.; Pohrivchak, M.A. *Some Wave-Theoretic Problems in Light Scattering and Radiative Transfer*; Light Scattering Reviews 11; Springer Praxis Books; Springer: Chichester, UK, 2016; pp. 339–361.
38. Kamke, E. *Differential Gleichungen*; Chelsea Publishing Co.: New York, NY, USA, 1948; Volume I, p. 440.
39. Nomura, Y.; Takaku, K. Tohoku Research Institutes. *Res. Inst. Elec. Comn.* **1955**, *7B*, 107.